Correlation Fourier diffractometry for long-pulse neutron sources: a new concept

Anatoly M. Balagurov[1], Valery A. Kudryashov[2]

[1]Frank Laboratory of Neutron Physics, JINR, Dubna, Russia, e-mail: bala@nf.jinr.ru
[2]Petersburg Nuclear Physics Institute, Gatchina, Russia, e-mail: vkudryashov@pnpi.spb.ru

Abstract

The extremely high resolution in large *d*-spacing range at relatively short flight path is the most positive result application of the correlation technique (pseudorandom or Fourier) in neutron diffractometry. The reverse time-of-flight Fourier (RTOF) method is especially promising after it has been developed to a high degree of perfection at a high-flux long-pulse neutron source, the IBR-2 reactor in Dubna, where the high resolution Fourier diffractometer (HRFD) has been constructed. The HRFD *d*-spacing resolution depends on the maximum frequency of neutron beam intensity modulation, amounts to the value of $\Delta d/d \approx 0.001$ in a wide d_{hkl} range (0.7 – 5 Å) for the flight path between the Fourier chopper and sample position as short as 20 m, and it can be improved, in principle, to $\Delta d/d \approx 0.0003$. The dominating problem that has been revealed during the operation of HRFD instrument is a complicated shape of diffraction lines, which could be asymmetric and usually displays small negative deeps on one or both sides of the diffraction peak. In the paper the experience of the HRFD operation at the IBR-2 pulsed reactor is analyzed and a possible solution of some technical problems is discussed. In addition, a new concept of the HRFD detector is suggested making it possible to considerably increase the detector solid angle.

1. Introduction

The resolution of a neutron TOF diffractometer mainly depends on the width of neutron pulse and the length of flight path. The resolution of high level, $\Delta d/d \approx 0.001$ or better, can be easily obtained at spallation sources of the ISIS type if a flight path amounts to 50 meters or longer. The main drawback of such instruments is too short *d*-spacing range, which is connected with pulse overlap problem. It can be overcome with the use of the correlation technique – pseudorandom [1] or RTOF-Fourier [2]; with both of that the very high resolution can be obtained at comparatively short flight path.

Although the correlation technique is known during many years, these methods are not widely spread and they are not very popular. Indeed, at continuous neutron sources (nuclear reactors) their application is not too effective because of a high level of "correlation background" which is proportional to the total amount of the scattered neutrons and independent of the time of flight. At spallation short-pulse sources such as ISIS or SNS, a conventional high-resolution TOF-diffractometer shows a lot of advantages, and nobody wants to replace it for the much more technically complicated and not so understandable Fourier diffractometer.

Nevertheless the potentials of correlation technique are good enough and especially it is related to the Fourier method, which allows to optimize the intensity-resolution ratio. The most promising is the construction of a Fourier-diffractometer at high-flux neutron source with pulse width of $\Delta t_0 > 300$ μs. Although at present only one long-pulse source – the IBR-2 reactor in Dubna is in real operation, there exist plans to construct the future ESS and may be the second target station at SNS as long-pulse neutron sources with Δt_0 about or even longer than 10^3 μs.

In this paper, the most important results obtained during operation of the high-resolution Fourier diffractometer (HRFD) at the IBR-2 reactor and its current status are reported, and possible solutions for some technical problems is discussed. In addition, a new concept of the HRFD detector is suggested making it possible to considerably increase the detector solid angle and the ideas for improving of the HRFD resolution and peak shape correction are presented. These improvements may transform the Fourier technique into the most prospective one for construction of neutron diffractometer with extremely high resolution ($\Delta d/d \approx 0.0003$) at long-pulse sources.

2. A schematic representation of the Fourier diffractometry

The Fourier method is based on modulation of the neutron beam intensity by the fast Fourier chopper, which consists of the rotating disk (rotor) and the stationary part (stator) with the same modulation pattern of radial sectors transparent and non-transparent for thermal neutrons (Fig. 1). The idea to use the Fourier chopper for a significant increase in the efficiency of diffraction experiment appeared in the beginning of 1970-ies [3]. It was shown that at fixed frequency of intensity modulation the transmission function of the chopper can be roughly represented as $Q_c(t) \sim 1 + \sin \omega t$ and there are two main contributions to the measured intensity: the first one is proportional to the Fourier harmonic of the coherent elastic scattering cross-section and the second one does not depend on neutron energy and is proportional to the total number of scattered neutrons. Performing measurements at varied frequencies (with discrete or continuous distribution) one can reconstruct scattering cross-section of a powder sample. The final pattern consists of narrow peaks (diffraction lines) and constant background, which is often referred to as a correlation background.

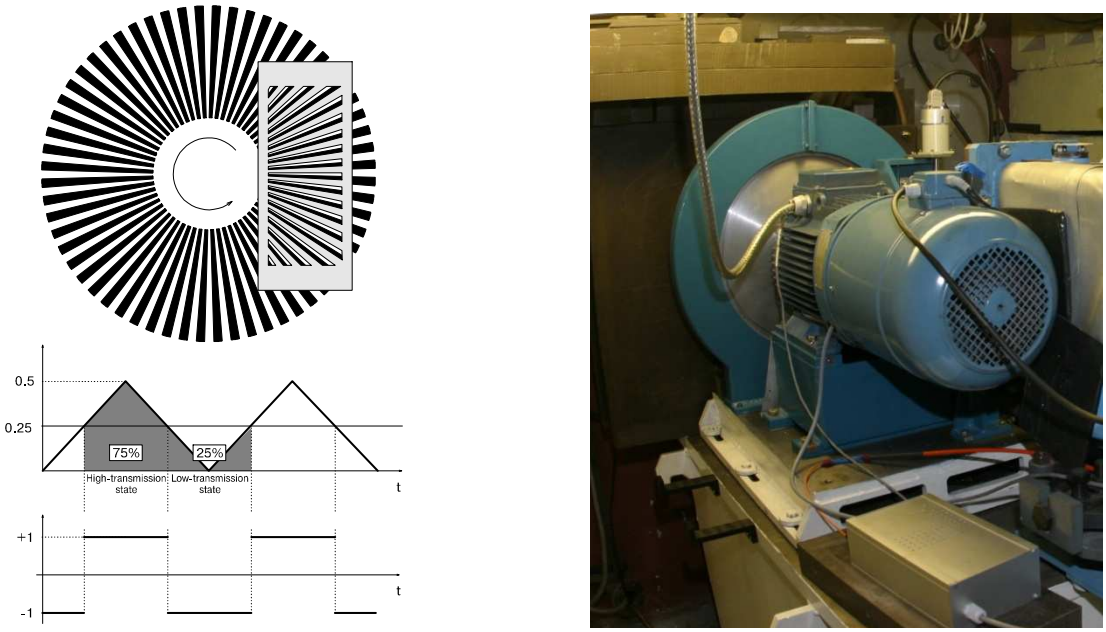

Fig. 1. On the left: The Fourier chopper schematic representation, including a rotor with transparent and nontransparent for thermal neutrons strips and a fixed stator. At the bottom, the chopper transmission function and the corresponding binary signals for the RTOF analyzer are also shown. On the right: The Fourier chopper picture. The revolving disk (∅50 cm) in the shroud and the motor (7.5 kW) are seen. The stator is situated at the right side of the disc.

Technical troubles related to the necessity for very high degree of chopper speed stabilization hampered the realization of the baseline idea. Successful practical realization of the neutron Fourier-diffractometry became possible after the so-called reverse time of flight (RTOF) method of data acquisition was introduced by Finnish physicists [4]. The basic idea of the RTOF method is an on-line check, for each detected neutron, of whether the registration probability is high or low. The check is realized by reverse analysis of neutron source and Fourier chopper states at the time the neutron passed through the corresponding points of the flight path. By carrying out neutron detection with the chopper speed continuously changing according to the particular law, and recording only those neutrons with a high probability of registration in the analyzer's memory, one can get the TOF distribution of elastically scattered neutrons, *i.e.*, the conventional TOF diffraction pattern.

This design can be realized at both steady state reactor [5] and at pulsed neutron source [2], for which the measured neutron intensity can be presented (in simplified form) as:

$$I(\tau) \sim \pm\int R_s(\tau-\tau')R_c(\tau-\tau')\sigma(\tau')d\tau' + c\int R_s(\tau-\tau')\sigma(\tau')d\tau' + B(\tau), \qquad (1)$$

where R_c is the resolution function of the Fourier chopper, R_s is the function describing the neutron pulse from the source, σ is the coherent scattering cross section of the sample, B is the conventional background, and c is some constant close to 1. For a perfect crystal for which $\sigma \sim \Sigma\delta(\tau - \tau_{0i})$, where τ_{0i} corresponds to the Bragg peak positions, and if the width of the function R_c is noticeably less than the width of R_s, i.e., $W_c << W_s$, the first term in (1) represents a narrow peak with a width close to W_c and the second term also describes a peak-like distribution, but with the width of the peaks close to W_s. The last is the correlation background in the case of pulsed source. By recording simultaneously $I(\tau)_+$ and $I(\tau)_-$ by two analyzers and subtracting them one can obtain high resolution diffraction pattern without wide peaks from the source (Fig. 2). The sum of $I(\tau)_+$ and $I(\tau)_-$ is (approximately) distribution of dispersions for high resolution pattern.

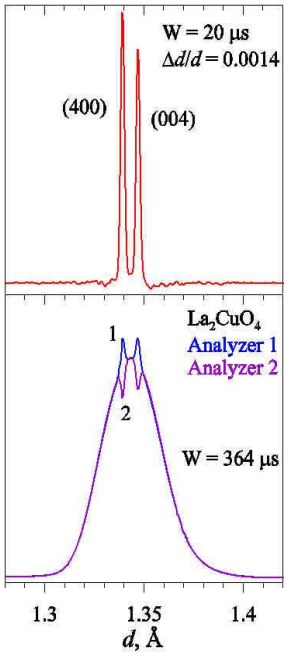

Fig. 2. A part of the diffraction pattern from La_2CuO_4 containing (400)/(004) reflex. At the bottom, the spectra measured by two analyzers, consisting of broad and narrow maxima, are shown. The upper part is obtained after subtraction of Analyzer-2 from Analyzer-1 showing the high resolution pattern with $\Delta d/d = 0.0014$.

The correlation background depends essentially on the width of the neutron pulse from the source and roughly can be presented as an integral of the neutron flux on the sample over the wavelength range $\Delta\lambda$ equivalent to W_s:

$$B \sim \int R_s(\tau - \tau')\sigma(\tau')d\tau' \sim \int_{\Delta\lambda} \Phi(\lambda)d\lambda = \Phi(\lambda)\Delta\lambda. \qquad (2)$$

where $\Phi(\lambda)$ is the wavelength distribution of the neutron flux on the sample. At the Fourier diffractometer at a steady state reactor, the correlation background does not depend on λ and is proportional to the total neutron flux on the sample. Accordingly one can estimate the ratio of the total flux and $\Phi(\lambda)\Delta\lambda$ (Fig. 3), which shows the decrease of correlation background for a pulsed source. This effect is especially huge at the low-intensity parts of the spectrum.

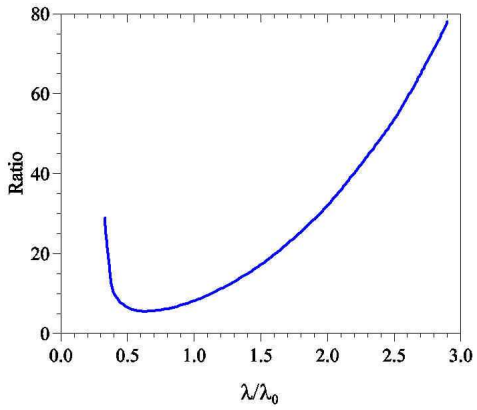

Fig. 3. The ratio of the correlation background in the Fourier diffractometer at a steady state and a long pulse neutron sources. The pulse width of LPS corresponds to the wavelength uncertainty $\Delta\lambda \approx 0.02\lambda_0$, where λ_0 is the parameter of the Maxwellian distribution.

Calculation of the resolution function for HRFD is the same as for conventional TOF diffractometer for powders:

$$R = \Delta d/d = [(\Delta t_0/t)^2 + (\Delta\theta/\mathrm{tg}\theta)^2 + (\tau_0/n)^2 + (\Delta L/L)^2]^{1/2}, \qquad (3)$$

where Δt_0 is the effective width of the neutron pulse, $t = 252.778L\lambda$ is the total time of flight (in μsec), L is the flight path from the source (Fourier chopper) to the detector (in m), λ is the wavelength of the neutron (in Å), θ is the Bragg angle, τ_0 and n are the width and number of channels of the TOF analyzer. The first term is the time-of-flight uncertainty, the second includes all the geometrical uncertainties connected with scattering at different angles, Δ means the full width at half maximum. For limited linear size of sample, detector with thin registration layer, and TOF analyzer with small enough channel width the contributions of the third and fourth terms in (3) are usually small in comparison with the first two.

The first term in (3) can be written as

$$R_t = \Delta t_0/t = \Delta t_0/(252.778\ L\lambda) = \Delta t_0/(505.556\ Ld\sin\theta), \qquad (4)$$

where Δt_0, L and λ or d are expressed in microseconds, meters, and Å, correspondingly. It can be shown that relation is valid:

$$R(t) \approx \Omega^{-1}\int_0^{\Omega} g(\omega)\cos(\omega t)d\omega, \qquad (5)$$

where $g(\omega)$ is the distribution of modulation frequencies of the neutron beam, which are distributed between zero and maximal value Ω. For maximal chopper rotation frequency ν_{max} and number of chopper transparent slits N, Ω is equal to $2\pi \cdot N \cdot \nu_{max}$. The width of $R(t)$ can be roughly estimated as $2\pi/\Omega$, and thus $\Delta t_0 \approx 2\pi/\Omega$ is effective pulse width, which must be used in (3). For ν_{max} = 150 Hz and N = 1024 (designed parameters of Fourier chopper at HRFD) one can obtain that $\Delta t_0 \approx 7$ μs. For this Δt_0 and flight path L = 20 m the TOF component of the resolution function is about 0.00035 (if d = 2 Å). This is nearly 2 times better than for conventional TOF diffractometer at 100 m flight path at the ISIS-type neutron source. Since the effective neutron pulse does not depend on wavelength, the R_t is proportional to $1/d$.

The geometrical part of the resolution function, $R_\theta = \Delta\theta/\mathrm{tg}\theta$, depends mainly on collimation of the incident neutron beam, sample and detector sizes. For the backscattering geometry, i.e. θ close to 90°, the R_θ can be quite small and roughly the same as R_t. The best compromise between solid angle of detector and its contribution to the resolution can be obtained if the time focusing conditions are satisfied [6].

3. High Resolution Fourier Diffractometer at the IBR-2 pulsed reactor

The pulse nature of the IBR-2 reactor in Dubna is provided by mechanical modulation of its reactivity, the pulse width is around 215 μs for fast neutrons, ≈340 μs for thermal neutrons and it is practically independent on neutron energy. Constructed by collaboration of FLNP (Dubna), PNPI (Gatchina), and VTT (Espoo, Finland), the High Resolution Fourier Diffractometer (HRFD) is intended mainly for structural studies of powders. The first high resolution diffraction patterns were obtained in 1992 [7] and regular operation of HRFD was started in 1995. The original design, principle of operation, and working parameters of the HRFD are described in details in paper [8]. HRFD upgrading was reported at ICANS conferences [9, 10] as well.

At present HRFD (Fig. 4) is situated at the beam-line with comb-like water moderator. In future at the modernized IBR-2M reactor at this beam-line the combined moderator consisting of warm (water) and cold (mesitylene at 30 – 50 K temperature) parts will be used. This will lead to the increase of the total flux by a factor of 2 and for the cold neutrons with λ > 4 Å by more than 10 times, and also to the more uniform spectral distribution of the incident beam.

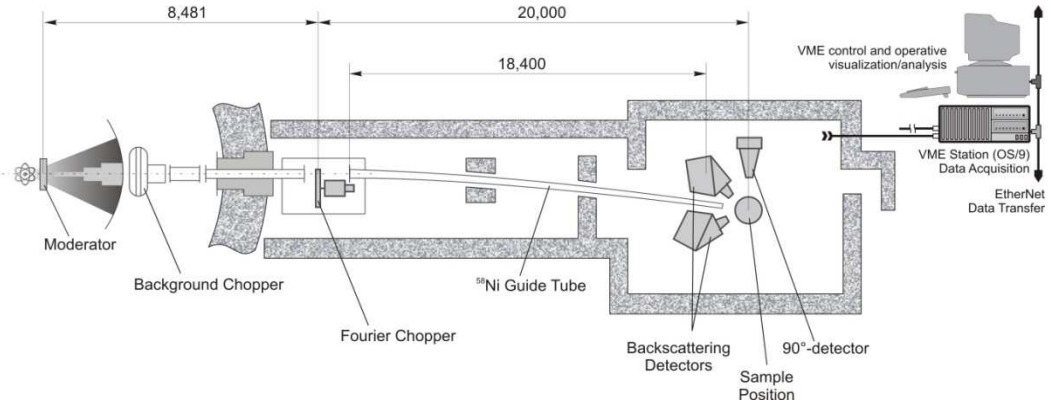

Fig. 4. The lay-out of HRFD at the IBR-2 pulsed reactor. The most important functional units are indicated. The distance between Fourier-chopper disk and sample position is exactly 20,000 mm.

For real polycrystalline sample with some level of microstresses and with limited size of coherently scattered domains the dependence of the diffraction peak width on d-spacing is:

$$W^2 = C_1 + C_2 d^2 + C_3 d^2 + C_4 d^4, \qquad (6)$$

here C_1 and C_2 are constants connected with the resolution function (3), which can be refined from data obtained with standard sample, $C_3 \sim (\Delta a/a)^2$ and $C_4 \sim 1/l_{cr}^2$ are connected with microstress and domain size, correspondingly. It is illustrated by Fig. 5, where one can see that for standard samples Al_2O_3 and $Na_2Al_2Ca_3F_{14}$ (NAC), for which the C_3 and C_4 coefficients are very small, the dependence of W^2 on d^2 is indeed the linear function. For the $CaCuMn_6O_{12}$ powder the larger slope of the line is connected with microstresses in this material (the C_3 coefficient is not small), while for fine-crystalline Ni the size effect is important.

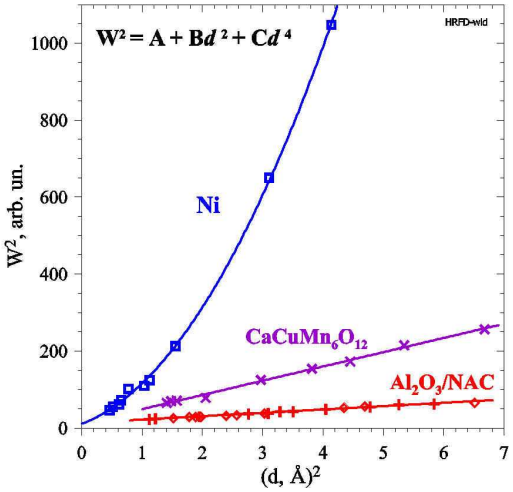

Fig. 5. Dependences of peak width on *d*-spacing, measured at HRFD. The bottom curve was measured with Al_2O_3 (crosses) and NAC (diamonds). It corresponds to the HRFD resolution function. In the $CaCuMn_6O_{12}$ powder, noticeable microstrains are present. For the fine Ni powder ($\langle d \rangle \approx 380$ Å), the size effect is evident.

The C_1 constant in (6) can be reliably determined from dependence of diffraction peak width on maximal speed of the Fourier chopper, $V_m \sim 1/\Omega$, as $C_1 \sim \Delta t_0 \sim 1/V_m$. In Fig. 6 the corresponding function, measured at HRFD, is shown. It is seen that the experimental data fairly correspond to calculation. It can be conclude also that, in principle, the TOF contribution to the resolution function could be as small as ~0.0002 at $d = 2$ Å, if Fourier chopper speed would be increased to $\sim 11 \cdot 10^3$ rpm and flight path elongated to ~30 m.

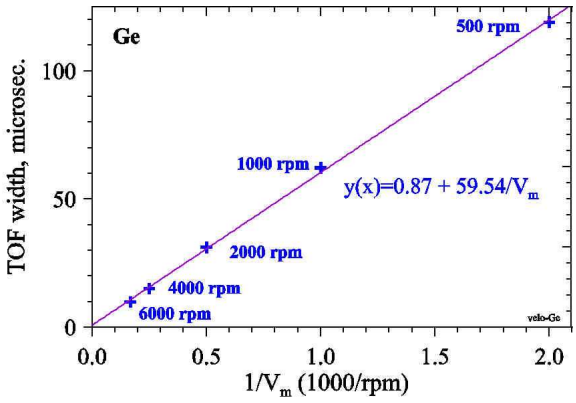

Fig. 6. TOF contribution in the full width as a function of $1/V_m$. The points were measured at maximal Fourier chopper speed from 500 to 6000 rpm. The experimental points (Ge powder) and least-square fit (continuous line) are shown.

The intensities of diffraction lines measured with HRFD can be described by the same formulae as for the conventional TOF diffractometer and consequently the Rietveld method can be used for their analysis. The analysis is somewhat more complicated due to the unusual peak shape, which becomes evident for high statistics (Fig. 7). As it was established, the peak shape depends on the frequency distribution of intensity modulation, adjustment of the pick-up signal phase, counts correlations in the neighboring TOF channels, and can be asymmetric, contain some negative deeps, or show both these features. To overcome this problem, the specialized program package MRIA [11] has been developed, which includes the possibility to use experimentally measured two-sign peak-shape model. The processing of data obtained with standard samples (Al_2O_3, NAC) shows good coincidence between experimental and calculated profiles (Fig. 8), as well as between the obtained from HRFD structural parameters and the literature data.

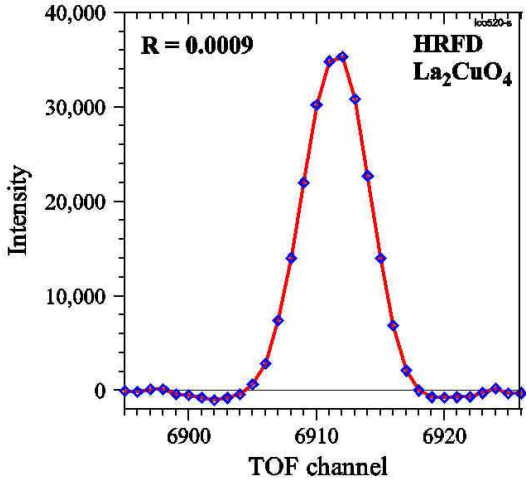

Fig. 7. A typical Bragg peak for a La_2CuO_4 single crystal measured at V_m = 6000 rpm with the TOF channel width of 2 μs. The relative width (Δn/n, n is the channel number of TOF analyzer) of this peak is about 0.0009. Small negative deeps on both sides of the peak are discussed in the next section.

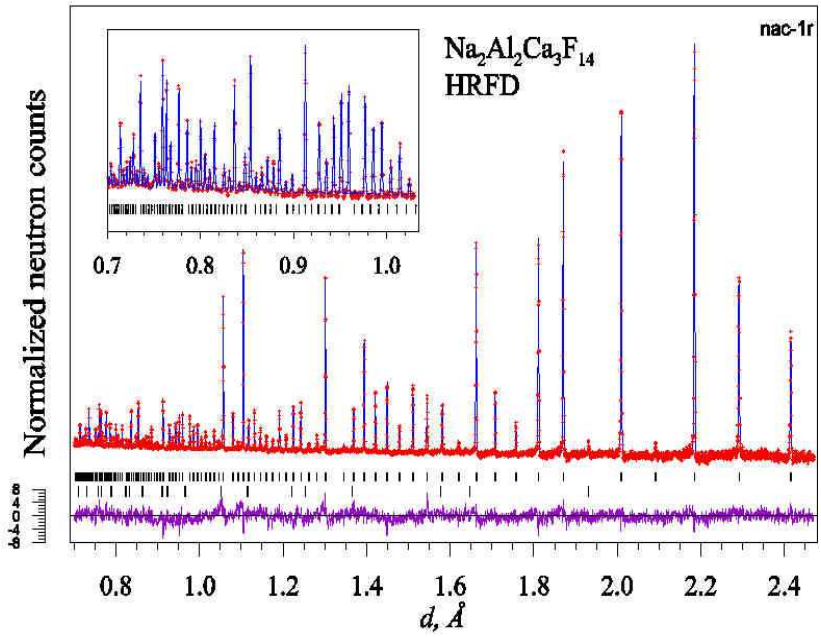

Fig. 8. The diffraction pattern of the NAC sample (with CaF_2 impurity phase) measured at V_m = 6000 rpm and processed by the Rietveld method. The difference curve is normalized on the mean-square deviation.

During last years the structures of various compounds have been studied at HRFD: the high-temperature superconductors (Y-123, Hg-1201, La_2CuO_{4+x}), hydrogen containing materials (Li_2BeD_4, $CeNi_3D_x$, $Ni(OH)_2$), complex perovskite-like oxides ($A_{1-x}A'_xMnO_3$, A_2GaMnO_{5+x}, $Ca(Cu,Mn)_7O_{12}$), various inorganic compounds ($LiCsSO_4$, $Sr_{11}Re_4O_{24}$, K_3PO_4). The short review of HRFD's scientific results is published in Ref. [12]. Until the appearance of the Fourier stress diffractometer (FSD) at the IBR-2 pulsed reactor, the HRFD was also used for the macro- and microstresses determination in bulk materials and components. Besides, the HRFD high resolution helps to measure the anisotropic peak broadening connected with non-spherical shape of crystallites (Fig. 9).

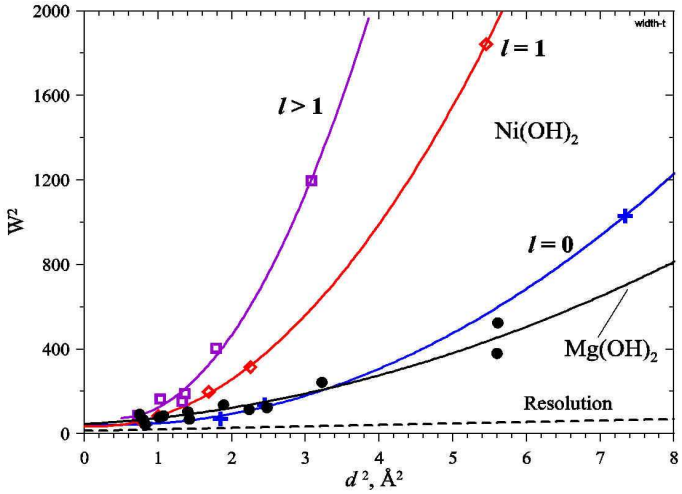

Fig. 9. Dependence of width of diffraction peaks of β-$Ni(OH)_2$ (for different values of *l*-index) and $Mg(OH)_2$ (for all *hkl*) as a function of d_{hkl}. Solid lines correspond to approximation of experimental points by 4 order polynomial, dashed line is resolution function. Contrary to the $Mg(OH)_2$, there is a strong dependence of β-$Ni(OH)_2$ peak widths on *l* indices, which is connected with small size of coherent domains along *c*-axis. The analysis shows that domains have disk-like shape with dimension in basic plane about 400 Å and in perpendicular direction about 150 Å.

4. Analysis of a peak-shape problem

As it was mentioned, one of the most pressing problem for HRFD is the complicated peak shape of the measured diffraction lines, which is mainly connected with TOF part of the resolution function, $R_\tau(\tau)$. In principle, the transmission function $X^{(\omega)}(t)$ and correctly phased pick-up signal $Y^{(\omega)}(t)$, shown in Fig. 1, must provide the "Gaussian" shape of the $R_\tau(\tau)$ function. But the simplified relation (5) is valid if two basic conditions are fulfilled:

- there is no phase mismatch, δ, between $X^{(\omega)}(t)$ and $Y^{(\omega)}(t)$,
- there is no amplitude distortion in frequency window, $g(\omega)$.

For analyzing these conditions let us write the more general and correct relation for $R_\tau(\tau)$ (details see in Refs. [13-16]):

$$R_\tau(\tau) = \frac{1}{C} \cdot \sum_{r=1}^{\infty} \left[\cos(\delta r) \cdot a_r \cdot F_C(r\tau) + \sin(\delta r) \cdot b_r \cdot F_S(r\tau) \right] \qquad (7)$$

Here C is normalization constant, δ is phase mismatch between $X^{(\omega)}(t)$ and $Y^{(\omega)}(t)$, a_r are the Fourier harmonics for the $X^{(\omega)}(t)$ and $Y^{(\omega)}(t)$ for $\delta = 0$, b_r are the same, but for $\delta = \pi/2$. The $F_C(r\tau)$ and $F_S(r\tau)$ functions are defined as:

$$F_C(r\tau) = \int_0^{\Omega} g(\omega)\cos(\omega r\tau)d\omega \qquad (8)$$

and

$$F_S(r\tau) = \int_0^{\Omega} g(\omega)\sin(\omega r\tau)d\omega \qquad (9)$$

In practice, two values of δ are important:

- $\delta \approx 0$, $R_\tau(\tau)$ is even and close to the $F_C(r\tau)$ function, which can be a Gaussian;
- $\delta \approx \pi/2$, $R_\tau(\tau)$ is odd and close to the $F_S(r\tau)$ function, which can be the first derivative of a Gaussian.

For $\delta \approx 0$ the second term in (7) can be considered as a small distorting factor and vice versa for $\delta \approx \pi/2$ the distortion of the peak shape are connected with the first term in (7).

For the triangle-like transmission function $X^{(\omega)}(t)$ and square-like pick-up signal function $Y^{(\omega)}(t)$ (as it is shown in Fig. 1), the coefficients a_r and b_r are:

$$a_r = \frac{1}{r^3}\cdot\sin(r\pi/2), \qquad (10)$$

$$b_r = \frac{1}{r^2}\cdot\sin^2(r\pi/2), \qquad (11)$$

For these a_r and b_r the first three harmonics (r = 1, 3, 5) for both terms in (7) are shown in Fig. 10. The resolution function $R_\tau(\tau)$ in this case is very close to the Gaussian function with distortions not more than 3% for δ = 0. If there exists any phase mismatch, the additional distortions would be proportional to $tg(\delta)$.

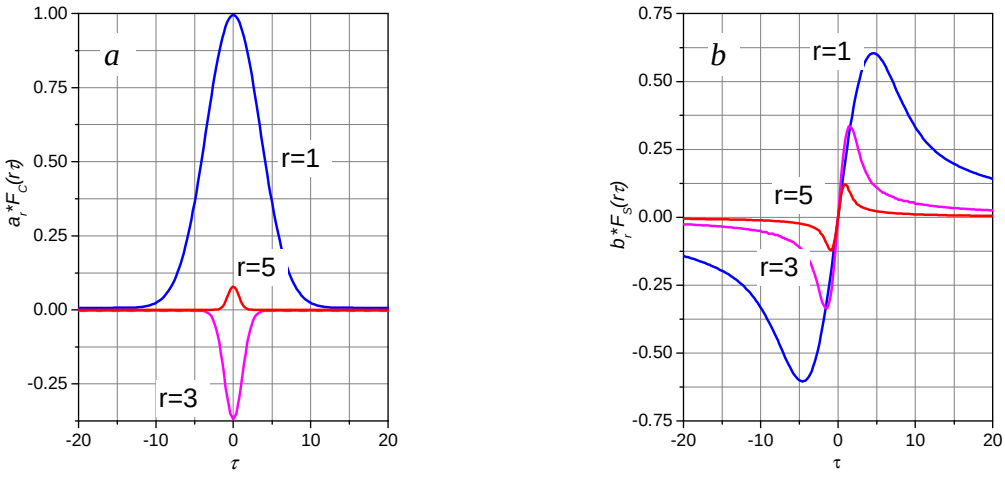

Fig. 10. (*a*) The term $a_r \cdot F_C(r\tau)$ in formula (7) for the TOF part of the resolution function $R_\tau(\tau)$. The members with r = 1, 3, 5 are shown (for r = 3 and 5 the coefficient 10 was introduced). (*b*) The term $b_r \cdot F_S(r\tau)$ in formula (7) for $R_\tau(\tau)$. The members with r = 1, 3, 5 are shown (for r = 3 and 5 the coefficient 5 was introduced).

Unfortunately, the perfect phase synchronism between $X^{(\omega)}(t)$ and $Y^{(\omega)}(t)$ is hard to be achieved. Moreover, as it results from our experience there is a long-term (weeks range)

instability in the magnitude of the phase mismatch. The effect of the phase mismatch is shown in Fig. 11, where the results of model calculations for $R_t(\tau)$ are presented. One can see that for $\delta \neq 0$ the peak shape becomes asymmetric. By eye this effect is visible if $\delta \approx 0.1$ rad (≈6°) or more. From this, the acceptable value of angle error (Δ) in the position of the pick-up signal transducer can be estimated. Taking into account that δ is related to the 2π period of the $X^{(\omega)}(t)$ and $Y^{(\omega)}(t)$ functions and the number of periods for one chopper rotation in our case is equal to 1024, it can be obtained that Δ must be smaller than $\delta/(2\pi \cdot 1024)$. It means that the asymmetry of the $R_t(\tau)$ would not be seen if $\Delta \leq 1.5 \cdot 10^{-5}$ rad ≈ 3″. Realization of so high stability of mechanical units is not simple task at present.

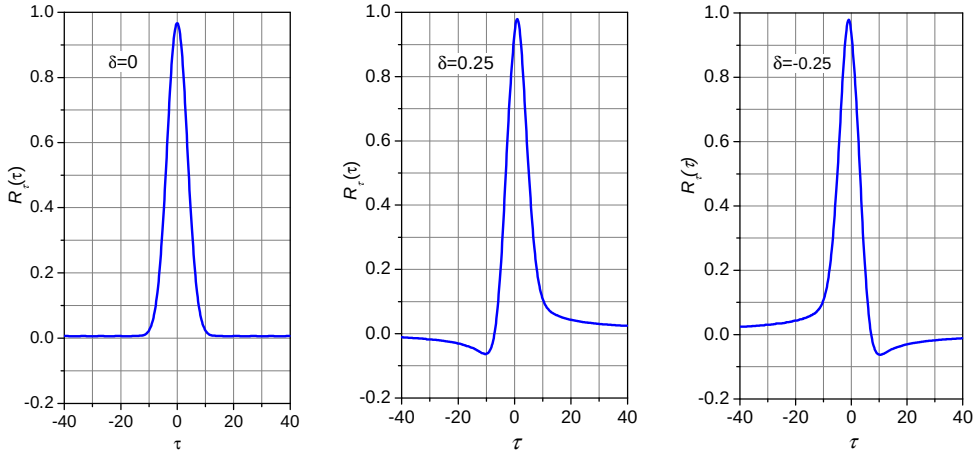

Fig. 11. The TOF part of the resolution function $R_t(\tau)$ calculated according (7) for three values of phase mismatch δ (0, 0.25, -0.25). It was supposed that the frequency window is exactly corresponding to $g(\omega)$.

As it follows from the formula (7), in addition to "phase" distortions the $R_t(\tau)$ function the "amplitude" distortions can affect the peak shape. They are connected with the aberration of the frequency window $g(\omega)$ from the expected distribution. For instance, one of the reasons of this aberration is the dependence of the transmission of the Fourier chopper on its speed (Fig. 12). The change of transmission is superimposed with $g(\omega)$, which leads to the decrease of the contribution of high frequencies and is accompanied by the increase in the peak width.

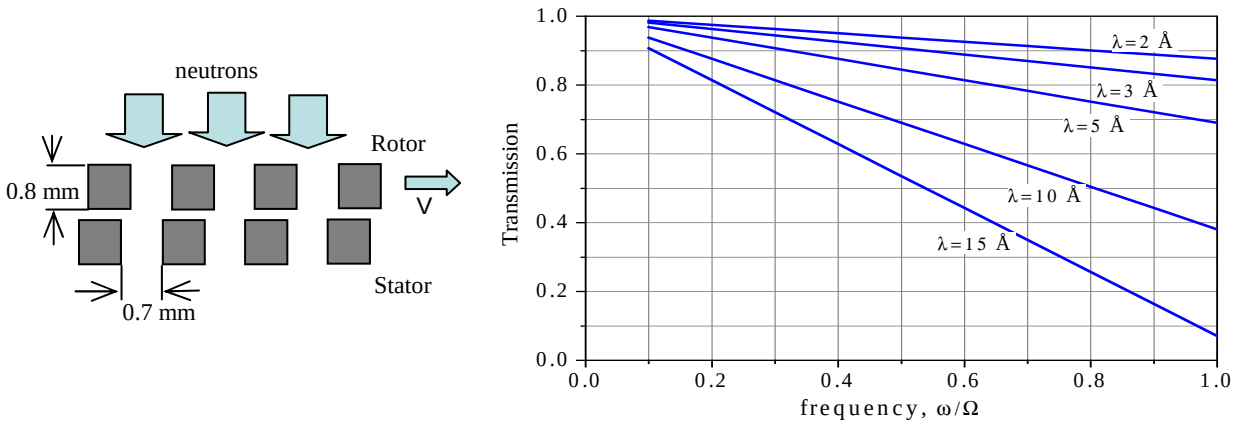

Fig. 12. The "collimation" effect of narrow rotating slits leads to the dependence of the transmission function on rotation frequency and neutron wavelength.

As it is demonstrated in Fig. 7 diffraction lines measured with high statistics contain the negative deeps at both sides. The model calculation shows that such peak shape is realized if the

contribution of low frequencies in $g(\omega)$ is slightly suppressed. As an example in Fig. 13 the peak with the negative deeps is shown, which was calculated for distribution $g_a(\omega) = g(\omega)\cdot(k\omega/\Omega + p)$ with k = 0.75 and p = 0.25. The additional factor $(k\omega/\Omega + p)$ just suppresses the lowest frequencies as it is shown by red curve in Fig. 14. In practice it can be connected with non-zero dead-time of the electronic system.

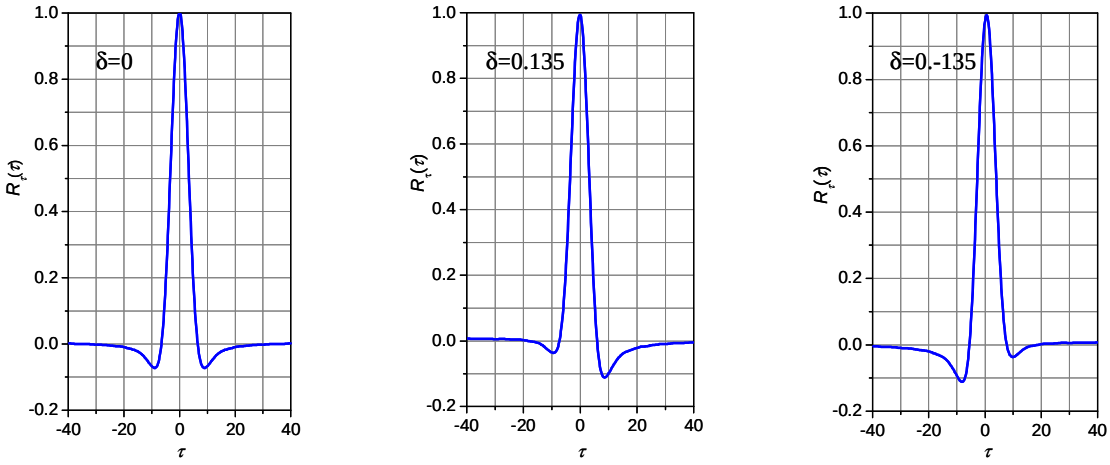

Fig. 13. The TOF part of the resolution function $R_t(\tau)$ calculated according (7) for three values of phase mismatch δ (0, 0.135, -0.135). Instead of the frequency window $g(\omega)$ the function $g(\omega)\cdot(0.74\omega/\Omega + 0.25)$ (shown in Fig. 14) was used for calculations.

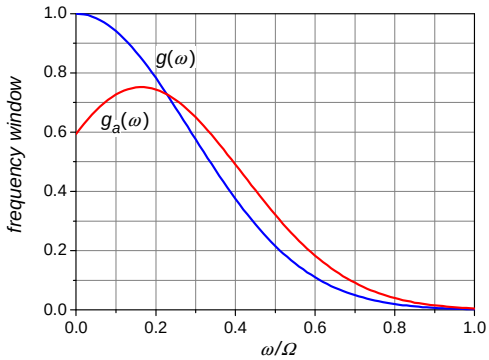

Fig. 14. The frequency window $g(\omega)$ (blue curve) providing the Gaussian peak shape. By the red curve the $g_a(\omega) = g(\omega)\cdot(0.74\omega/\Omega + 0.25)$ function with suppressed low frequency part is shown.

This peak-shape problem could be solved if the so called “list-mode” (time stamped) data acquisition system is used. In this mode, the electronics assigns to the each detector count several identifiers and the absolute time passed from the start of the experiment. As identifiers are written in the two 32 bits words and include detector element number, indicators for chopper pick-up signal passing up and down, indicator of the source start pulse, and indicators of experiment start and finish. One of the function of the second word is extending of the time counter up to $1\cdot10^6$ seconds.

In contrast to the existing on-line analyzer, no real diffraction pattern is written in memory. In the list-mode, the absolute time of a detector count is fixed with high precision (32 nsec) and is written together with indicators of an event as raw data on the disk. Also, any number of independent detector elements can be included in the system, which is important for the detectors with large solid angles. Besides, the list-mode offers the possibility the subsequent data processing by introducing of various algorithms. In particular, the phase shift of the pick-up signal can be calculated and inserted; any deviation from specified frequency window can be

fixed etc. Thus, the new system of Fourier data acquisition makes it possible a posteriori correction of the peak shape.

5. New HRFD BS detector: maintaining resolution for larger solid angle

To ensure high intensity, it is necessary to have a large solid angle of the detector and, at the same time, its geometrical contribution to the resolution function must not exceed the TOF component to secure a high-resolution capability. At present the HRFD back-scattering (BS) detector system includes two banks located symmetrically relative to the incident neutron beam at mean scattering angles of ±152°. Each detector consists of 32 scintillation plates of the NE902 type of 1 mm thickness. The total area of both detectors is equal to 0.48 m^2, which corresponds to 0.2 sr solid angle. The plates are situated on surface of rotation around the beam axis in accordance with time focusing condition. From the resolution point of view this detector is fully satisfying the desired conditions, but its solid angle is certainly too small to be state-of-the-art.

A new wide-aperture BS detector (Fig. 15) for HRFD with solid angle of about 1.5 sr is under construction now. The detector has the ring-like structure; each ring is divided on several independent sections (166 sections), which cover the total area of 13.5 m^2. The ZnS(Ag)/^{6}LiF scintillation screens of 0.42 mm thickness with wavelength shifting fibers readout are used as detector elements. Being flexible, the scintillation screen allows each element of the detector to approximate the time focusing surface (TFS) for the scattered neutrons with necessary accuracy. The design of the detector is based on our experience in construction of the multi-element detectors with combined geometrical-electronic focusing for FSD instrument at the IBR-2 reactor [17].

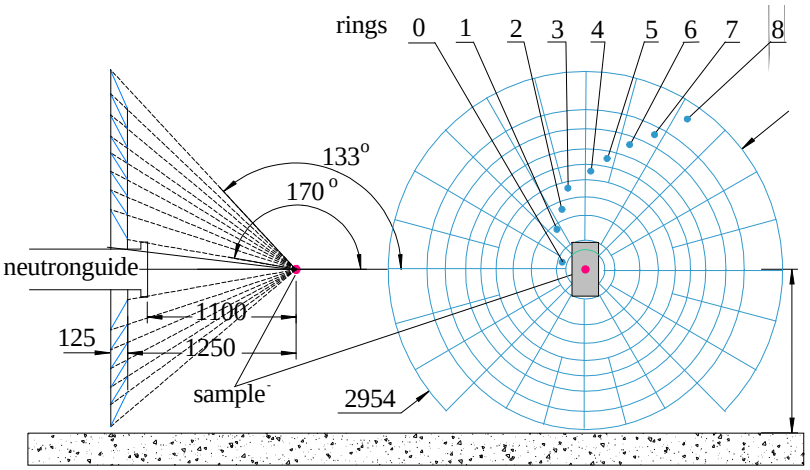

Fig. 15. The schematic view of the new ZnS(Ag)/^{6}LiF back-scattering detector (side and front view). Detector consists of 8 rings, divided on 166 elements. Each element is focused geometrically. The total solid angle of the detector is close to 1.5 sr, the whole screen area is equal to 13.5 m^2.

The sensitive layer of each detector element is well tailored to the particular TFS, which is characterized by individual parameters depending on the solid angle Ω_R, Bragg angle θ_R, and incidence angle α_R for neutrons striking the screen. Diffraction patterns measured by the detector rings will be electronically focused into the same time-of-flight scale using recently developed technique [18]. The uncertainties in the flight path ($\Delta L_\eta/L$, η is number of a ring) arising due to the inaccuracy in matching of the screen and TFS and the screen thickness are the main factors defining the detector contribution to the resolution function. The principal problem in the accurate matching of the screen and TFS originates from the possibility to bend a screen only in one direction, while TFS is curved in two perpendicular directions (saddle-point surface). In Fig.

16, the parameter $2.35\sigma_\eta=\Delta L_\eta/L$ is illustrated for all detector rings for several sample dimensions. One more important factor that should be taken into account is the dependence of the detector efficiency on the ring number (Fig. 17), which is connected with difference in α_R parameters.

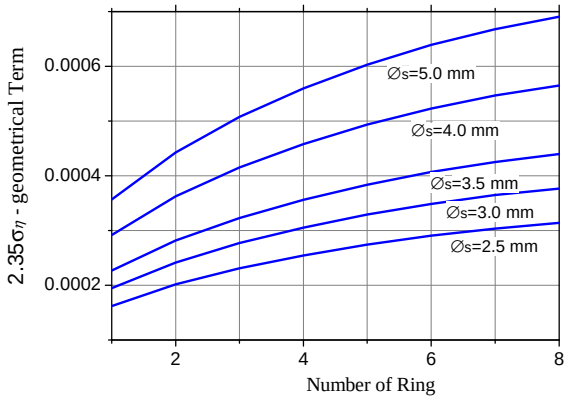

Fig. 16. The uncertainty of the flight path as a function of detector ring number and diameter of sample container.

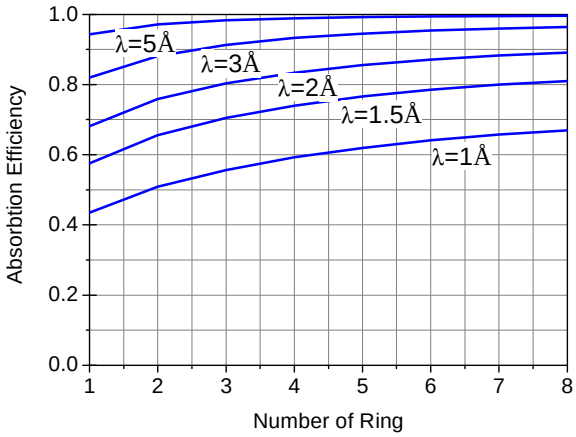

Fig. 17. Efficiency of neutron detection as a function of of detector ring number and neutron wavelength.

The geometrical contribution to the HRFD resolution function (3) is connected also with the incident beam divergence. This contribution varies from ring to ring due to the differences in the Bragg angles, θ_R. The beam divergence $\Delta\theta$ can be regulated by putting collimator before the sample. The simple calculations show that the geometrical contribution from the whole detector can be as small as $5\cdot10^{-4}$ if sample of 2.5 mm diameter and collimator with 2.5 mm slit and 1.1 m length are used.

6. Conclusions

The Fourier diffractometer, compared to a conventional TOF machine, ensures obtaining a very high resolution at a quite short flight path allowing the neutron flux to be increased and the cost of the instrument to be reduced. Also, it is important that its resolution (as for TOF mashine) only slightly depends on d_{hkl} being practically constant in the large d-spacing range. The pulse overlap problem, which is so upsetting for high resolution TOF-diffractometers with long flight paths, does not exist for the Fourier diffractometer.

From technical point of view the only additional unit of HRFD in comparison to a conventional TOF-diffractometer is a Fourier chopper with a motor control system, which is, in

principle, quite simple device. It should be noted also, that it does not require a synchronization of its rotation with the neutron source. The only pressing problem requiring special attention is a peak shape, which, as we hope, can be solved by introducing the list-mode of data acquisition.

With HRFD the resolution level of $9 \cdot 10^{-4}$ has been practically achieved for chopper – sample distance of 20 meters and chopper rotation speed of $6 \cdot 10^{3}$ rpm. The level of $3 \cdot 10^{-4}$ can be definitely achieved for slightly faster Fourier chopper (11,000 rpm) and a bit longer flight path (30 meters) at least for several internal rings of the new back-scattering detector. These improvements could transform the Fourier technique into the most prospective one for construction of neutron diffractometers with resolution of about 0.0003 at pulsed neutron sources. At least, this technique can be considered as the real alternative to the long-flight-path and to the multi-chopper diffractometers.

Acknowledgement

All the work discussed in the paper is the result of the effort of many people in FLNP (Dubna), PNPI (Gatchina), and VTT (Espoo, Finland) named in the references. During many years this work was partially financed under a JINR-BMBF (Germany) agreement.

References

1. U. Freudenberg, W. Glaser "A new pseudostatistical time-of-flight spectrometer for quasielastic neutron scattering studies" Nucl. Instr. & Methods, **A243** (1986) 429.
2. P. Hiismaki, H. Poyry, A. Tiitta "Exploitation of the Fourier chopper in neutron diffractometry at pulsed sources" J. Appl. Cryst., **21** (1988) 349.
3. A.C. Nunes, R. Nathans, B.P. Schoenborn "A neutron Fourier chopper for single crystal reflectivity measurements: some general design considerations" Acta Cryst., **A27** (1971) 284.
4. H. Poyry, P. Hiismaki, A. Virjo "Principles of reverse neutron time-of-flight spectrometry with Fourier chopper applications" Nucl. Instr. and Methods, **126** (1975) 421.
5. P. Hiismaki, V.A. Trounov, O. Antson, V.A. Kuryashov, H. Kukkonen, H. Poyry, A.F. Shchebetov, A.Tiitta, V.A. Ulyanov "Experience of the Fourier TOF neutron techniques for high-resolution neutron diffractometry" Neutron Scattering in The ′Nineties, Conf. Proc., p.453, Vienna, IAEA (1985).
6. J.M. Carpenter "Extended detectors in neutron time-of-flight diffraction experiments" Nucl. Instr. and Methods, **47** (1967) 179.
7. V.L. Aksenov, A.M. Balagurov, V.G. Simkin, Yu.V. Taran, V.A. Trounov, V.A. Kudrjashov, A.P. Bulkin, V.G. Muratov, P. Hiismaki, A. Tiitta, and O. Antson, "The new Fourier diffractometer at the IBR-2 reactor: design and first results" Proceedings of ICANS-XII, 24-28 May 1993, Abingdon, U.K., vol.1, I-124-131.
8. V.L. Aksenov, A.M. Balagurov, V.G. Simkin, A.P. Bulkin, V.A. Kudrjashov, V.A. Trounov, O. Antson, P. Hiismaki, A. Tiitta "Performance of the high resolution Fourier diffractometer at the IBR-2 pulsed reactor" J. of Neutron Research, **5** (1997) 181.
9. A.M. Balagurov "Recent developments of neutron diffraction instruments at the IBR-2 pulsed reactor" ICANS-XIV conference, ANL Proceedings 98/33, **2** (1998) 650.
10. A.M. Balagurov "New developments of TOF neutron diffraction at the IBR-2 pulsed reactor" ICANS-XV conference, KEK Proceedings 2000-22, **1** (2000) 504.
11. V.B. Zlokazov, V.V. Chernyshev "MRIA - a program for a full profile analysis of powder multiphase neutron-diffraction time-of-flight (direct and Fourier) spectra" J. Appl. Cryst., **25** (1992) 447.
12. A.M. Balagurov "High resolution Fourier diffraction at the IBR-2 reactor" Neutron News, **16** (2005) 8.

13. V.A. Kudryashov, H.G. Priesmeyer, J.M. Keuter, J. Schroder, R. Wagner, V.A. Trounov “Optimization of detectors in time-focusing geometry for RTOF neutron diffractometers” Nuclear Instruments and Methods in Physics Research, **B93** (1994) 355.
14. V.A. Kudryashov, H.G. Priesmeyer, J.M. Keuter, J. Schroder, R. Wagner “On the shape of the diffraction peaks measured by Fourier reverse time-of flight spectrometry” Nuclear Instruments and Methods in Physics Research, **B101** (1995) 484.
15. V.A. Kudryashov, H.G. Priesmeyer, J.M. Keuter, J. Schroder, R. Wagner “Phase errors and their influence on the RTOF-Fourier method” Nuclear Instruments and Methods in Physics Research, **B103** (1995) 517.
16. Pekka Hiismäki “Modulation Spectrometry of Neutrons with Diffractometry Applications” World Scientific Publishing Co. Pte. Ltd, 1997.
17. E.S. Kuzmin, A.M. Balagurov, G.D. Bokuchava, V.V. Zhuk, V.A. Kudryashov, A.P. Bulkin, V.A. Trunov “Detector for the FSD Fourier-diffractometer Based on ZnS(Ag)/^{6}LiF Scintillation Screen and Wavelength Shifting Fiber Readout” Journal of Neutron Research, **10** (2002) 31.
18. V.A. Kudryashov, V.A. Trounov, V.G. Mouratov “Improvement of Fourier method and Fourier diffractometer for internal residual strain measurements” Physica B, **234-236** (1997) 1138.